The dependence on microstructure of the magnetotransport behaviour in $Sm_{1/2}Sr_{1/2}MnO_3$

2002 J. Phys.: Condens. Matter 14 8853

(http://iopscience.iop.org/0953-8984/14/38/309)

INSTITUTE OF PHYSICS PUBLISHING JOURNAL OF PHYSICS: CONDENSED MATTER

J. Phys.: Condens. Matter **14** (2002) 8853–8860 PII: S0953-8984(02)26337-7

The dependence on microstructure of the magnetotransport behaviour in $Sm_{1/2}Sr_{1/2}MnO_3$

K M Gu[1], T Tang, Q Q Cao, Y Q Chen, J H Wang and S Y Zhang

National Laboratory of Solid State Microstructures, Department of Physics, Nanjing University, Nanjing 210093, People's Republic of China

E-mail: kmgu@sina.com

Received 28 June 2001, in final form 21 May 2002
Published 12 September 2002
Online at stacks.iop.org/JPhysCM/14/8853

Abstract

Two sets of polycrystalline manganites with the composition $Sm_{1/2}Sr_{1/2}MnO_3$ were prepared using the sol–gel (SG) and the solid-state reaction (SSR) methods. It is found that the magnetotransport properties for both sets of samples with the same composition are very strongly dependent on their preparation methods. For the SG samples, insulating behaviour at zero magnetic field over a temperature range from 70 to 300 K, and a metal–insulator transition with a huge reduction in resistance near $T_C \sim 100$ K under a sufficiently high magnetic field over 2 T, which lead to a maximum magnetoresistance ratio value up to 10^5% at 2 T and over 10^6% at 5 T near 65 K, were observed. However, for the samples prepared by the SSR method the resistance (R)–temperature (T) curve only showed a single insulator–metal transition. At the same time, their temperature-dependent magnetizations, $M(T)$, are also totally different. The morphologies obtained by scanning electron microscopy demonstrate that there is a large difference in microstructure between the two sets of samples. The fine grains and a large number of grain boundaries are primary factors leading to the insulating characteristics at zero field and the unique transport properties induced by a sufficient magnetic field in the SG samples.

1. Introduction

Interesting magnetic and transport properties of doped manganites $R_{1-x}A_xMnO_3$ (R: trivalent rare-earth ions, such as La, Pr, Nd, Sm; and A: divalent alkaline-earth ions, such as Ca, Sr, Ba, Pb) with perovskite structure have been investigated extensively since the discovery of colossal magnetoresistance (CMR). It has been reported that there is a fine interplay between magnetic, Coulomb, and lattice interactions in these compounds [1–3], leading to many phenomena such as ferromagnetism and the associated transition from insulator to metal

[1] Author to whom any correspondence should be addressed.

0953-8984/02/388853+08$30.00

Table 1. Comparison of values of $\langle r_A \rangle$ and σ^2.

Compounds	$\langle r_A \rangle$ (Å)	σ^2 (Å^2)
$La_{0.5}Sr_{0.5}MnO_3$	1.40	0.0016
$Pr_{0.5}Sr_{0.5}MnO_3$	1.37	0.0049
$Nd_{0.5}Sr_{0.5}MnO_3$	1.355	0.0072
$Sm_{0.5}Sr_{0.5}MnO_3$	1.34	0.0100
$Pr_{0.5}Ca_{0.5}MnO_3$	1.32	0.0004

near the Curie temperature T_C, the CMR effect, and charge ordering. The magnetic and transport properties in these compounds are dependent on the effective d-electron hopping interaction and the one-electron bandwidth W, which is controlled by changing the Mn–O–Mn bond angles (or the composition of the A-site cations). On the basis of the value of W, the manganites can be divided into large-, intermediate-, and low-bandwidth compounds [4]. For example, $La_{1-x}Sr_xMnO_3$ (LSMO) is considered to be representative of the 'large'-bandwidth perovskites, and has a higher Curie temperature T_C and a wide ferromagnetic metallic phase region within the composition range between $x = 0.17$ and 0.48 [4]. Normally, the CMR effect near T_C for the perovskite compounds can be interpreted on the basis of the double-exchange mechanism. $Nd_{1-x}Sr_xMnO_3$ (NSMO) and $Pr_{1-x}Sr_xMnO_3$ (PSMO) are typical perovskites with intermediate bandwidth due to the presence of a stable charge-ordered (CO) phase at $x = 0.5$. Their CO state can be easily destroyed by a magnetic field in a first-order transition [4]. $Pr_{1-x}Ca_xMnO_3$ (PCMO) is one of the low-bandwidth manganites, which presents a particularly stable CO state in a broad composition region between $x = 0.3$ and 0.75. For example, the critical magnetic field needed to destroy the CO state at 4.2 K in NSMO ($x = 0.5$) is about 11 T, and for PSMO ($x = 0.5$) about 5 T. A lot of experiments have shown that the manganites with intermediate to low bandwidth show the largest CMR effects.

Recently, a phase separation model has been widely used for manganites in order to interpret curious transport properties [4–8]. According to this model, different phases coexist in single-crystal samples with a percolative characteristic, and the state of phase separation determines the properties of the materials. Therefore, in most manganites the insulating phase is at least as important as the metallic phase and the boundary between the metal and the insulator is the most interesting region as regards achieving a large-magnetoresistance (MR) effect [4]. At some critical point, such as $x = 0.5$, the percolative state of coexisting phases is sensitively dependent on conditions such as temperature, pressure, and magnetic field. This makes it difficult to get a reliable estimate of effective transport properties such as the dc resistivity ρ_{dc} of the samples. $Sm_{1/2}Sr_{1/2}MnO_3$ provides an example.

$Sm_{1-x}Sr_xMnO_3$ is an intermediate-bandwidth manganite due to large average A-site cationic radius $\langle r_A \rangle$ and the higher mismatch of A-site cation size, $\sigma^2 = \Sigma x_i r_i^2 - \langle r_A \rangle^2$ (here x_i and r_i are the fractions and radii for A-site ions, respectively). For the sake of comparison, table 1 gives values of $\langle r_A \rangle$ and σ^2 for several compounds with $x = 0.5$. It is seen from table 1 that for $Sm_{0.5}Sr_{0.5}MnO_3$ $\langle r_A \rangle = 1.35$ Å which is close to that for NSMO and $\sigma^2 = 0.01$ Å^2 which is the maximum value among all the manganites. Normally, $Sm_{0.5}Sr_{0.5}MnO_3$ should present similar transport properties to $Nd_{0.5}Sr_{0.5}MnO_3$. In fact, several research groups have studied the magnetic and transport properties of the $Sm_{1-x}Sr_xMnO_3$ system, but have given several contradictory results [9–13]. Martin *et al* [10] prepared the polycrystalline compound with $x = 0.5$, and found there is just a peak is observed around T_C in the resistance (R)–temperature (T) curve, corresponding to a transition from the paramagnetic insulator (PMI) to the ferromagnetic metal (FMM). Kasai *et al* [11] studied magnetic and magnetotransport

properties of the $Sm_{1-x}Sr_xMnO_3$ films. They found that for the films with $x = 0.55$, the zero-field resistivity increases as temperature decreases—similar to the case for a typical insulator—and under a magnetic field of 2, 3, or 4 T, their R–T curve shows a clear thermal hysteresis, indicating the existence of a first-order phase transition. With magnetic field increased up to 5 T, the thermal hysteresis disappears. Tomioka *et al* [13] measured the temperature dependence of the zero-field resistivity of the single crystal $Sm_{1/2}Sr_{1/2}MnO_3$, and found that it is a typical insulator, similar to the film. To elucidate such a distinct difference in transport properties of $Sm_{1/2}Sr_{1/2}MnO_3$, it is important to explore the origin of this difference and the relationship between microstructure and transport behaviour. For this purpose, for this paper a series of polycrystalline $Sm_{1/2}Sr_{1/2}MnO_3$ samples were prepared using the conventional solid-state reaction (SSR) method and the sol–gel (SG) method, and the effect of the microstructure on the magnetic and transport properties was studied systematically.

2. Experimental details

Some of the samples under investigation were prepared by the SG technique. An appropriate amount of citric acid (as a complex agent) and glycol (as a dispersing agent) were added into a solution which was previously obtained by dissolving the high-purity oxides Sm_2O_3, $SrCO_3$, and $Mn(NO_3)_2$ in dilute nitric acid. The gel was then decomposed slowly at $\sim$200 °C in air. This precursor was decarbonated at 700 °C for 6 h, then the powder obtained was ground, pelletized, and sintered at 1100 °C for 10 h. Finally, pellets were sintered again at 1200 or 1300 °C for 10 h without an intermediate grinding and furnace-cooled down to room temperature.

Another group of samples with the same composition were prepared by the conventional SSR method using high-purity oxides (Sm_2O_3, $SrCO_3$, and Mn_3O_4) with an intermediate grinding and a final sintering process at 1300 °C for 10 h in air. At the final stage of the sintering process all the samples were cooled down to 800 °C at a rate of 5 °C min^{-1} and then some of the samples were quenched in air (samples A) while some were furnace-cooled (samples B).

X-ray diffraction (XRD) and scanning electron microscopy (SEM) were employed to investigate the microstructure of the samples. The dc resistance was measured in the temperature range of 40–300 K using a standard dc four-probe method. The MR ratio was defined as $MR = [\rho(0) - \rho(H)]/\rho(H)$ and was measured in a superconducting magnetic field up to 7 T. Magnetization versus temperature measurements were performed from 10 to 150 K in a LakeShore vibrating-sample magnetometer under magnetic fields of 10^{-2} and 2 T. The composition of the samples was analysed using the inductively coupled plasma (ICP) quantometer technique.

3. Results and discussion

The powder x-ray diffractograms of the SG samples and SSR samples show orthorhombic perovskite structure (figure 1). The ICP analysis confirmed that the components in SG samples are Sm:Sr:Mn = 0.507:0.493:0.991; this is close to their nominal composition and that of the SSR samples. In addition, the density values for both samples were measured using the Archimedes method. The sintering temperatures, 1200 °C for the SG samples and 1300 °C for the SSR samples, were so chosen that the relative difference in density between the samples was controlled within 4% about 6 g cm^{-3}.

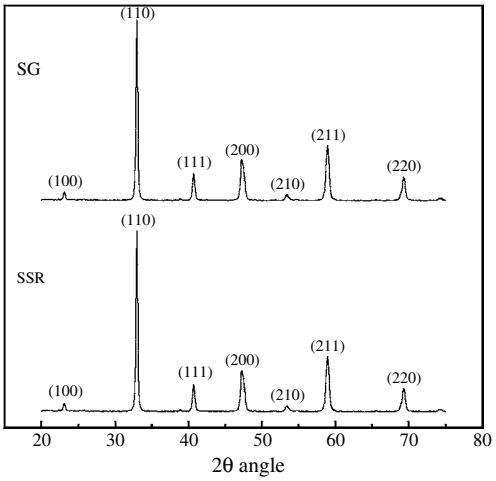

Figure 1. XRD patterns of polycrystalline samples of $Sm_{1/2}Sr_{1/2}MnO_3$ prepared by the SG and SSR methods.

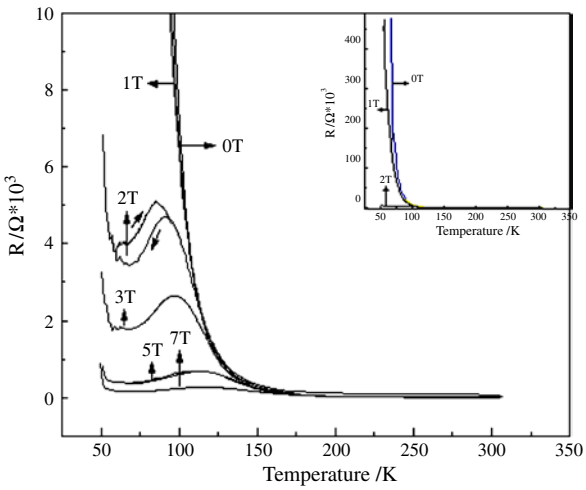

Figure 2. The temperature dependence of the resistance of $Sm_{1/2}Sr_{1/2}MnO_3$ prepared by the SG method; the inset shows the comparison of the resistances of samples under magnetic fields of 0, 1, and 2 T.

(This figure is in colour only in the electronic version)

Figure 2 shows the R–T curve of the SG sample. The measurements of the resistances of samples with the same sizes indicate that the resistivity of the SG samples is larger than that of the SSR samples at room temperature. The value of the room temperature resistance for SG samples sintered at different temperature is different, but the shapes of the R–T curves are similar. The zero-field resistance, as shown in figure 2, increases with decreasing temperature, exceeding the measurement limit of 10^6 Ω at about 70 K, showing that insulator characteristics and no metal–insulator transition are observed throughout the temperature region. By applying a sufficiently high magnetic field over 2 T, a huge reduction in resistance is induced near T_C of about 100 K, indicating a metal–insulator transition induced by the magnetic field—therefore,

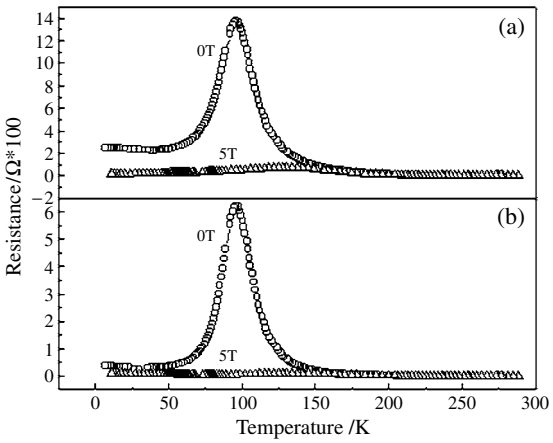

Figure 3. The temperature dependence of the resistance of $Sm_{1/2}Sr_{1/2}MnO_3$ prepared by the SSR method: (a) cooled by a quenching process; (b) cooled slowly.

giving rise to an obvious CMR effect. The sample exhibits a FMM state down to another temperature called T^*, of 65 K, below which the sample becomes an insulator again. At the magnetic field of 2 T, the R–T curve shows a thermal hysteresis in the temperature range from T_C to T^*, indicating the occurrence of a first-order phase transition. The thermal hysteresis disappears as the magnetic field is increased to as high a value as 5 T, perhaps reflecting an increase in the carrier itinerancy [11]. The insulating state still exists even at a very high magnetic field of 7 T. With increasing magnetic field, T^* shifts to lower temperature while T_C moves oppositely. A maximum MR value over $10^6\%$ is obtained at 5 T near $T^* \sim 65$ K. Even at 2 T, the MR value is still as large as $10^5\%$. It is noted that this MR value at 5 T is an order of magnitude larger than that of the SSR samples and almost the same as that of the $Sm_{0.45}Sr_{0.55}MnO_3$ films reported by Kasai *et al* [11]. Their films were prepared on a substrate of (100) $SrTiO_3$ using pulsed laser deposition (PLD). The zero-field resistivity of these films increases with decreasing temperature, suggesting the existence of an insulating state in the films. On applying magnetic fields, as shown in figure 2 for the $x = 0.5$ bulk SG sample, a huge reduction in resistivity, an induced metal–insulator transition, and a clear thermal hysteresis in the resistivity versus temperature are also observed. But there is a clear difference between the R–T curves of bulk SG sample and those of the films. The resistivities of the former increase drastically once again (see figure 2), while those of the latter tend to a constant value smoothly under a sufficiently high magnetic field, for example $\geqslant 3$ T, with temperature decreasing further, below 75 K. This suggests that the SG sample presents a remarkable transition from a FMM state to an antiferromagnetic insulating (AFMI) state, while the films do not transform so obviously as the SG sample at lower temperature.

For SSR samples there were two sets of samples (A and B) to be prepared, corresponding to quenching and furnace-cooling to room temperature from 800 °C in the process of cooling after finishing the sintering at 1300 °C, respectively, in order to find out the effects of the final cooling stage in the sintering process on the transport properties. Figure 3 shows their R–T curves at the magnetic fields of 0 and 5 T. Their MR values are about $10^5\%$ at 5 T near $T_C \sim 100$ K. Here no resistance jump, i.e., no FMM–AFMI transition, occurs at lower temperature. It is obvious that the effect of quenching from 800 °C at the final stage of sintering increases only the zero-field resistance and the MR value at lower temperature below 150 K, and has little influence on T_C and transport characteristics.

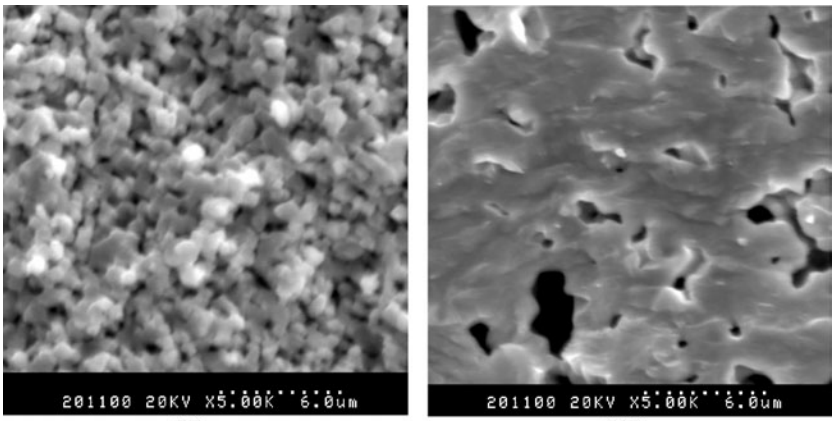

Figure 4. SEM morphologies of samples prepared by the SG method and SSR method. The two samples were sintered at 1300 °C for 10 h.

It is found from figures 2 and 3 that the SG samples with the same nominal composition obviously differ from the SSR samples in their transport behaviour. The microstructures of both the samples were observed by SEM in order to investigate the reasons for the difference. Figure 4 shows their SEM morphologies. It is obvious that the SG sample is composed of fine equiaxial grains with the size (diameter) of 0.4–0.6 μm, while the SSR sample has a relatively dense microstructure, containing large elongated grains with long semi-axes of 2.5–3.0 μm and short semi-axes of about 0.5 μm. If the two grain types are regarded as a prolate ellipsoid of revolution and a sphere, respectively, it is estimated that the mean volume of one grain in the SSR sample is 45 times as large as that of one in the SG sample. In view of the granularity of the SG samples, the volume fraction of grain boundaries in the SG samples is much greater than that for the SSR samples.

In general, experimental and theoretical studies on phase separation in manganites show that in the compounds near $x = 0.5$ two states coexist—for example, a FMM state and an AFMI state. Their transport properties are governed by the competition of the metallic and the insulating state. It can be seen from the magnetic phase diagram of the $Sm_{1-x}Sr_xMnO_3$ system [10] that the $x = 0.5$ compound lies in the transition zone, sandwiched between the FMM and AFMI domains. Near $x = 0.5$ the CO temperature, T_{CO}, increases with x, from ~140 K for $x = 0.4$ up to 205 K for $x = 0.6$, and is lower than T_C. Hence, for the $x = 0.5$ compound the measurements of the magnetic and transport behaviour should indicate the coexistence of two magnetic transitions with decreasing temperature, that is, PMI–AFMI and AFMI–FMM. However, the experimental results measured for the SSR samples and SG samples are totally different. For $x = 0.5$ SSR samples, it is found that, as Martin *et al* [10] pointed out, only a bump is observed on the M–T curves corresponding to the PM–AFM transition. The M–T curves measured for the SSR samples are similar to that given by Martin *et al* (see figure 6 of [10]). The M–T curves for the SG sample are shown in figure 5. It is obvious that as temperature decreases, a bell-shape M–T curve is obtained for the SG sample. Its right-hand side corresponds to the transition from the PMI state to the FMM state, while its left-hand side corresponds to one from the FMM state to the AFMI state. This is in agreement with the expectation from the phase diagram mentioned above.

In the following the reason for the great difference in transport behaviour between the SSR and SG samples is discussed briefly.

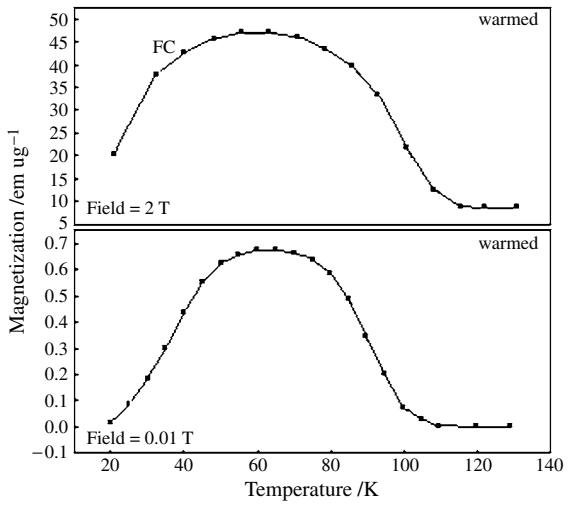

Figure 5. The temperature dependence of the magnetization of the SG sample, under magnetic fields of 10^{-2} and 2 T.

It is well known that the disordered region in perovskite manganites has a great effect on the magnetic and magnetotransport properties. This arises in two ways: one is from the great difference in A-site cation radius between the single crystal and the grains; the other is from the grain boundaries in polycrystals. According to the review by Dagotto *et al* [4], phase separation in manganites can be divided into electronic and disorder-induced types. The former takes place between phases with different concentrations and leads to nanometre-scale coexisting clusters, while the latter has characteristics of percolation between equal-density phases, driven by disorder near the first-order metal–insulator transition, and is even more promising than the electronic type as regards explaining the physics of manganites. Dagotto *et al* [4] pointed out that if the couplings are the same, but the strength of the disorder is so large that it becomes dominant, then tiny clusters of two competing phases are formed with the lattice spacing as the typical length scale. $Sm_{1/2}Sr_{1/2}MnO_3$ should provide an example due to it having the largest σ^2-value (see table 1) and, thus, stronger disorder. Hence, it can be speculated that for our SG and SSR samples a phase separation can occur. As a consequence, two competing phases, FMM and AFMI, coexist in the grains in the form of tiny clusters. The R–T curves shown in figure 3 for the SSR samples containing large grains seem to be compatible with the expected resistivity versus temperature in the percolative picture because of the large resistivity at 0 K.

The second form of disordered region is the grain boundaries in polycrystals. Recently, the effect of grain boundaries in bulk polycrystalline manganites has been studied intensively [14–16]. It is believed, generally, that the grain boundaries are insulating with high resistivity due to the disordered ion distribution and not sensitive to change in outside conditions, while the transport properties of grains can be easily affected by many factors such as temperature and magnetic field. The large number of grain boundaries for the SG samples with fine grains will greatly increase the volume fraction of insulating state, which separates the metallic phases into islands isolated from each other. Because grain boundaries are insulating and the SG samples contain a lot of grain boundaries, it is impossible to form the percolative route of the metallic state, leading the samples to exhibit an insulating transport behaviour. An applied magnetic field can help to connect adjacent preformed metallic clusters that were originally

separated by an insulation barrier or to improve the conductivity of insulator phases, hence leading to an increase in the proportion of metallic phase [17]. When a crucial proportion in the percolative regime is reached under a sufficiently high magnetic field, a transition from insulator to metal occurs, inducing an enormous change in resistivity. For our SG sample, the magnetic field obviously affects the transport behaviour is 2 T. At even lower temperature, the transition from the FM state to the insulating state for SG samples can be attributed to two factors. One is that the dynamic energy of the hopping electrons decreases and the other (more important) is that the AFM phase that existed originally becomes stronger in the competition with the FM phase as temperature is decreased. As seen in figure 5, the slow reduction of the magnetization M with decreasing temperature below 75 K suggests that the AFM phase in the SG sample becomes predominant; therefore, the sample is an insulator again, resulting in a steep rise of the resistance at lower temperatures in figure 2. A stronger applied magnetic field favours the metallic phases, thus making T^* shift to lower temperature.

4. Conclusions

In summary, we have investigated the relationship between microstructure and effective magnetotransport behaviour in polycrystalline samples of $Sm_{1/2}Sr_{1/2}MnO_3$. Our results show that the fine grains and large number of insulating grain boundaries in the samples along with the details of the preparation method play important roles in determining the magnetotransport behaviour. Polycrystalline manganite with the same composition, $Sm_{1/2}Sr_{1/2}MnO_3$, can display significantly different magnetotransport behaviour and a different CMR effect.

Acknowledgments

This work was supported by the National Key Project for Basic Research G 1999064508, and by the NSFC, No 19890310 (4), China.

References

[1] Chahara K, Ohno T, Kasai M and Kozono Y 1993 *Appl. Phys. Lett.* **63** 1990
[2] Jin S, Tiefel T H, McCormack M, Fastnacht R A, Ramesh R and Chen L H 1994 *Science* **264** 413
[3] Uhlenbruck S, Teipen R, Klingeter R, Büchner B, Friedt O, Hücker M, Kierspet H, Siemoller D, Pinsard L, Revcolevschi A and Gross R 1999 *Phys. Rev. Lett.* **82** 185
[4] Dagotto E, Hotta T and Moreo A 2001 *Phys. Rep.* **344** 1–153
[5] Moritomo Y 1999 *Phys. Rev.* B **60** 7921
[6] Uehara M, Mori S, Chen C H and Cheong S-W 1999 *Nature* **399** 560
[7] Rhyne J J, Kaiser H, Luo H, Xiao G and Gardel M L 1998 *J. Appl. Phys.* **83** 7339
[8] Lopez J, Lisboa-Filho P N, Passos W A C, Ortiz W A and Araujo-Moreira F M 2000 *Preprint* cond-mat/0004460
[9] Damay F, Maignan A, Martin C and Raveau B 1997 *J. Appl. Phys.* **81** 1372
[10] Martin C, Maignan A, Hervieu M and Raveau B 1999 *Phys. Rev.* B **60** 12 191
[11] Kasai M, Kuwahara H, Tomioka Y and Tokura Y 1996 *J. Appl. Phys.* **80** 6894
[12] Tokura Y, Kuwahara H, Moritomo Y, Tomioka Y and Asamitsu A 1996 *Phys. Rev. Lett.* **76** 3184
[13] Tomioka Y, Kuwahara H, Asamitsu A and Kasai M 1997 *Appl. Phys. Lett.* **70** 3609
[14] Hwang H Y, Cheong S-W, Ong N P and Battlogg B 1996 *Phys. Rev. Lett.* **77** 2041
[15] Steenbeck K, Eick T, Kirsch K, Schmidt K H-G and Steinbeiß E 1998 *Appl. Phys. Lett.* **73** 250
[16] Gross R, Alff L, Büchner B, Freitag B H, Höfener C, Klein J, Lu Yafeng, Mader W, Philipp J B, Rao M S R, Reutler P, Ritter S, Thienhaus S, Uhlenbruck S and Wiedenhorst B 2000 *J. Magn. Magn. Mater.* **211** 150
[17] Fåth M, Freisem S, Menovsky A A, Tomioka Y, Aarts J and Mydosh J A 1999 *Science* **285** 1540